

Article

Selective Flotation Separation of Chalcopyrite from Copper-Activated Pyrite and Pyrrhotite Using Oxidized Starch as Depressant

Guangxing Bai ¹, Chunyuan Huang ¹, Yonghao Li ^{2,*} and Ming Zhang ^{2,*}

¹ Daye Iron Mine Co., Ltd., WISCO Resources Group, Huangshi 435006, China; dayeironbai@126.com (G.B.); dayeironhuang@163.com (C.H.)

² School of Resources and Environmental Engineering, Wuhan University of Science and Technology, Wuhan 430081, China

* Correspondence: yonghaoli@wust.edu.cn (Y.L.); m.zhang@wust.edu.cn (M.Z.)

Abstract: The disadvantages of using lime to depress the flotation of copper-activated pyrite and pyrrhotite are well known. In this study, oxidized starch, prepared by the ozone nanobubble technology, was employed as an eco-friendly depressant for copper-activated pyrite and pyrrhotite in the flotation of chalcopyrite. Single mineral flotation showed that oxidized starch inhibited the flotation of copper-activated pyrite and pyrrhotite at pH 5.5 while having no significant impact on chalcopyrite flotation. Zeta potential and adsorption measurements, together with XPS analysis and EDTA extraction, were conducted to understand the mechanism underpinning the selective depression behavior of oxidized starch. It was found that oxidized starch had a stronger affinity for copper-activated pyrite and pyrrhotite than for chalcopyrite. The depression of pyrite and pyrrhotite by oxidized starch was due to the combined effect of the formation of hydrophilic Cu-starch complex and the oxidation of Cu(I) on their surfaces. Further, oxidized starch was examined in the flotation of an actual bulk sulfur concentrate where a comparable depression performance to that of lime was shown. This investigation may contribute to the greening of the chalcopyrite flotation process by demonstrating the promising potential of oxidized starch for copper-activated pyrite and pyrrhotite depression.



Academic Editor: Hyunjung Kim

Received: 6 January 2025

Revised: 24 January 2025

Accepted: 26 January 2025

Published: 29 January 2025

Citation: Bai, G.; Huang, C.; Li, Y.; Zhang, M. Selective Flotation Separation of Chalcopyrite from Copper-Activated Pyrite and Pyrrhotite Using Oxidized Starch as Depressant. *Minerals* **2025**, *15*, 133. <https://doi.org/10.3390/min15020133>

Copyright: © 2025 by the authors. Licensee MDPI, Basel, Switzerland. This article is an open access article distributed under the terms and conditions of the Creative Commons Attribution (CC BY) license (<https://creativecommons.org/licenses/by/4.0/>).

Keywords: chalcopyrite; pyrite; pyrrhotite; segregation flotation; flotation depressants; starch; copper activation

1. Introduction

Pyrrhotite and pyrite are often found in association with magnetite and chalcopyrite iron (Fe)-copper (Cu) polymetallic deposits [1]. Pyrrhotite is known for its magnetic properties; magnetic pyrrhotite can be easily enriched in the concentrate during the magnetic separation process [2–4]. Meanwhile, flotation, a common method for separating valuable minerals from ores, has been adopted to recover pyrrhotite using xanthate collectors [5–8]. Therefore, a flotation first then magnetic separation flow sheet is normally adopted to concentrate Cu, sulfur (S) and Fe from this type of ore. In flotation, a bulk chalcopyrite-pyrrhotite-pyrite concentrate is firstly obtained by bulk sulfide flotation, followed by copper-sulfur separation with the aid of pyrite and pyrrhotite depressants [6,9]. However, the readily oxidized pyrrhotite possesses a low floatability. Copper ions are therefore added to boost pyrrhotite flotation in the bulk sulfide flotation stage [4,10–13], which makes its depression in the following Cu-S separation stage even more difficult.

Lime and cyanide have been the most widely used depressants for iron sulfide minerals in the conventional Cu-Fe sulfide flotation separation circuits because of their satisfactory depressive performance [14–16]. However, while the use of lime suffers from high lime consumption as well as scaling in pipelines [17], cyanide gradually fades out due to high toxicity [15,18–21]. Polyamines such as diethylenetriamine (DETA) have been proven to be effective in inhibiting the flotation of Cu^{2+} -activated pyrrhotite and pyrite [22–24]. However, DETA-metal complex as the dominant depression product is extremely stable and soluble in water, which can make the concentrations of metal ions such as Cu^{2+} in the backwater exceed that stipulated in regulations [23,25,26]. Therefore, eco-friendly iron sulfide depressants are urgently needed to achieve a cleaner and more efficient beneficiation of copper and iron minerals from the Fe-Cu polymetallic deposits.

Starch, a natural, widely available, non-polluting biopolymer, has previously been examined as a depressant for pyrite and pyrrhotite [15,25]. It is made of two major components: linear amylose and highly branched amylopectin [27]. However, while native starch struggled to cope with the ongoing decrease in grade and increase in mineralogy complexity of the ore deposits worldwide, starch modification by oxidation has the potential to meet this challenge [14,15,23,25,28]. For instance, Khoso et al. have successfully utilized a modified starch (tricarboxylate sodium starch) to separate chalcopyrite from pyrite and from pyrrhotite [15,29]. However, the pyrite and pyrrhotite used in their studies were pure minerals without pre-activation by copper ions. Fletcher et al. found that compared to the use of natural wheat starch, oxidized starch resulted in a better depression of Cu^{2+} -activated pyrite due to the introduction of $-\text{C}=\text{O}$ and $-\text{COOH}$ substituents, accompanied by depolymerization upon oxidation [28,30]. Unfortunately, only single mineral (pyrite) flotation was performed in their study. The feasibility of using oxidized starch for flotation separation of chalcopyrite from Cu^{2+} -activated pyrite and pyrrhotite is still not clear, which is the main focus of this study. It is worth mentioning that selective depression of iron sulfide using other natural polysaccharides including dextrin and guar gum [16], as well as several pretreatment technologies such as low temperature plasmas and Fenton oxidation, has also been documented [31].

Ozone is known for its environmentally friendly nature as there are no secondary pollutants produced in the oxidation process [32–34]. It has been reported that ozone has a higher solubility and a longer residence time in the aqueous phase when administered as nanobubbles (NBs) [35,36]. In this paper, ozone NB technology was adopted to prepare oxidized starch and the effect of ozone NB oxidized starch (ONOS) on the flotation behaviors of single copper-activated pyrite, pyrrhotite and chalcopyrite, as well as a bulk chalcopyrite-pyrrhotite-pyrite concentrate was investigated.

2. Materials and Methods

2.1. Materials and Reagents

Pure lump chalcopyrite, pyrite and pyrrhotite samples were received from Guangdong Province, China. The purity of chalcopyrite, pyrite and pyrrhotite was determined by X-ray diffraction (XRD) and chemical composition analysis and the results are shown in Figure 1 and Table 1, respectively. Each sample was first crushed by a hammer covered by hard plastic and then ground using a laboratory vibratory mill (HLXZM-100, Hengle Mineral Engineering Equipment, Wuhan, China). The milled samples were then dry screened to obtain $+38\text{--}74\ \mu\text{m}$ fraction for flotation tests, while the $-38\ \mu\text{m}$ fraction was used for adsorption tests, zeta potential and XPS and EDTA extraction. To minimize surface oxidation, the prepared samples were hermetically sealed and stored in a refrigerator. A bulk sulfur concentrate was collected from the Daye Iron Mine of WISCO (Huangshi, China). The mineralogical study shows that sulfur in the raw iron ore is mainly in the

form of sulfides (pyrite, pyrrhotite and chalcopyrite), while iron is mainly in the form of magnetite, as shown in Table 2. The bulk sulfur concentrate was obtained by a bulk flotation of the sulfides after copper-activation. The contents of copper and sulfur in the bulk sulfur concentrate were 5.02%, and 43.76%, respectively.

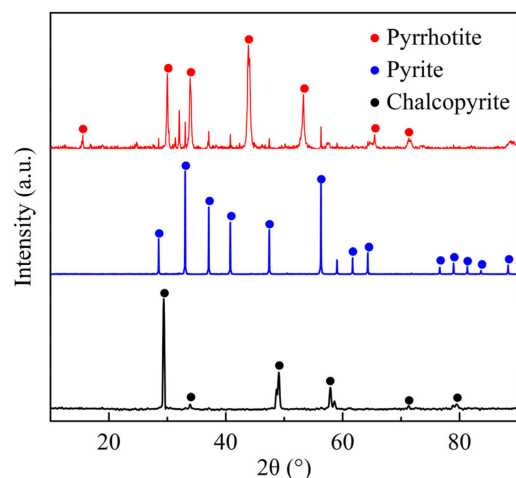


Figure 1. XRD analysis of the chalcopyrite, pyrite and pyrrhotite samples.

Table 1. Chemical composition of chalcopyrite, pyrite and pyrrhotite samples.

	Elements (wt.%)							
	Cu	Fe	S	Mg	Al	Si	Ca	P
Chalcopyrite	31.829	30.367	34.481	-	0.025	0.368	0.088	0.021
Pyrite	-	45.343	48.920	0.033	0.120	0.375	0.235	0.022
Pyrrhotite	0.124	52.019	34.115	0.726	0.189	1.465	1.010	0.019

Table 2. Mineral composition of the raw iron ore from Daye Iron Mine of WISCO.

Mineral	Magnetite	Pyrite	Chalcopyrite	Pyrrhotite	Muscovite
Content (%)	25	6	4	2	3
Mineral	Chlorite	Calcite	Tremolite	Diopside	Other
Content (%)	6	24	10	8	12

Potassium ethyl xanthate (KEX), isopropyl ethyl thionocarbamate (Z200) and terpineol were provided by Daye Iron Mine of WISCO. Corn starch was sourced from Weihaomei Food (Wuhan, China). NaOH, HCl, KCl, lime, sulfuric acid, phenol and ethylenediaminetetraacetic acid (EDTA) were all purchased from Sinopharm Chemical Reagent (Shanghai, China). Copper sulfate pentahydrate ($\text{CuSO}_4 \cdot 5\text{H}_2\text{O}$) was purchased from Macklin Biochemical Technology (Shanghai, China).

2.2. ONOS Preparation

A custom-made ozone NB oxidation system (Figure 2) based on the combination of hydrodynamic cavitation and ozonation was adopted for the preparation of ONOS [37]. In particular, a 3% (*w/v*) starch solution was prepared and transferred to the ozone NB preconditioning system and treated for 30 min, during which time the ozone gas concentration and flow rate were held at 45 ± 5 mg/L and 0.2 L/min, respectively. The treated starch solution was filtered and the residues were dried at 40 °C in a vacuum oven [34].

After grinding with a mortar and pestle, the dried starch was sieved with a 75 μm screen and sealed in plastic bags.

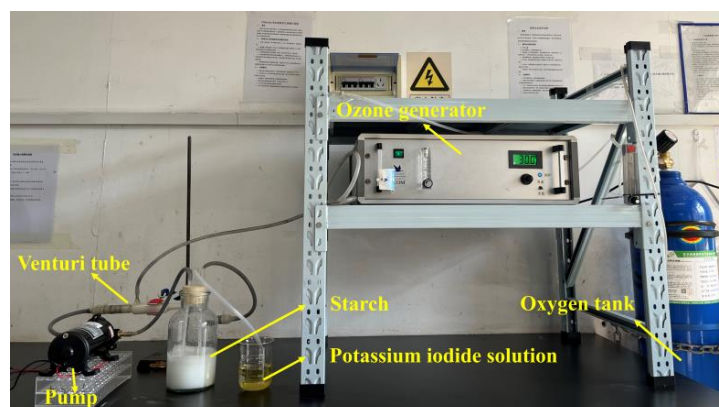


Figure 2. Setup of the ozone NB oxidation system used in this study.

2.3. Flotation Tests

Single mineral flotation tests were carried out on an XFGC flotation machine equipped with a 50 mL plexiglass cell and the agitation speed was maintained at 1680 rpm. For each test, 3 g of chalcopyrite/pyrite/pyrrhotite together with 40 mL of deionized water was added to the cell to make up the flotation pulp. The pulp was then mixed for 2 min, during which time the pulp pH was adjusted to the desired values using NaOH and HCl. After that, 300 g/t CuSO_4 , 600 g/t ONOS, 400 g/t KEX and 200 g/t terpeneol were added sequentially and conditioned for 2 min each. After manual scraping for 4 min, the concentrate and tailing were collected, dried at 80 $^\circ\text{C}$ for 12 h and weighed for recovery calculations.

2.4. Adsorption Tests

For each test, 1.0 g of mineral sample was added to a beaker containing 100 mL of deionized water to form a mineral slurry. The pH of the slurry was then adjusted to 5.5, followed by the addition of 3×10^{-4} mol/L CuSO_4 solution for 5 min and a predetermined dose of ONOS was added to the slurry with continuous stirring for 1 h. After that, 50 mL of the slurry was transferred to a centrifuge tube and centrifuged for 20 min at 4000 rpm. The residual concentration of starch in the supernatant was determined according to the method of Dubois [38]. Specifically, 2 mL of the supernatant was collected in a test tube, to which 0.05 mL of 80% *w/v* phenol solution and 5 mL of 98% sulfuric acid were added sequentially. Finally, the reaction solution was subject to a UV-Visible spectrophotometer (Shimadzu UV-2550, Duisburg, Germany) and measured at 490 nm [25].

2.5. Zeta Potential Measurements

The zeta potential measurements on Cu^{2+} -activated chalcopyrite, pyrite and pyrrhotite were conducted using a zeta sizer (Nano ZS90, Malvern Instruments, Malvern, UK). For each test, 200 mL of 1×10^{-3} mol/L KCl solution was added to a 250 mL baker as a background electrolyte solution, followed by the addition of 50 mg of mineral sample. The resulting suspension was then mixed for 5 min by a stirrer, during which time its pH was adjusted using dilute NaOH or HCl solution. Desirable amounts of CuSO_4 and ONOS were added sequentially and reacted for 5 min each. After settling for another 5 min, the supernatant was subjected to zeta potential measurements.

2.6. X-Ray Photoelectron Spectroscopy (XPS)

Surface analyses of pyrrhotite and pyrite were carried out using XPS. Samples were prepared following the same procedure as the flotation tests, except that KEX and terpeneol

were not added. The slurry was filtered, washed with deionized water thrice then dried in a vacuum oven at 30 °C. Background corrections were applied to the C 1s, Cu 2p, Fe 2p and O 1s spectra using the SMART method. Peak shapes were defined using the Gauss–Lorentz function. The C 1s binding energy peak at 284.8 eV was used for energy calibration.

2.7. EDTA Extraction

For each extraction, 180 mL of 3 wt.% EDTA solution was prepared and its pH was adjusted to 7.5 using NaOH. The EDTA solution was then added to a reaction vessel and flushed with argon gas for 10 min to eliminate oxygen. During this period, 20 mL of flotation pulp was freshly prepared following the procedure described in Section 2.3, except that KEX and terpineol were not added. The pulp was then transferred to the vessel and stirred continuously for 15 min while the argon gas flushing was maintained to prevent mineral oxidation [39,40]. After that, the pulp was filtrated with 0.45 µm membrane filter and the filtrate was subjected to ICP-OES analysis for copper, while the solid obtained was dried and weighed.

3. Results and Discussion

3.1. Flotation of Single Minerals

Figure 3 shows the flotation recovery of Cu²⁺-activated single chalcopyrite, pyrrhotite and pyrite as a function of flotation time at different pH conditions using 600 g/t ONOS as a depressant. Note that pH 5.5 was selected because it was the optimal pH for the depression performance of a similar oxidized starch (prepared with H₂O₂ and NaOH) in separating chalcopyrite from pyrite [29]. Both pyrrhotite and pyrite showed poorer floatability than chalcopyrite at all the three pHs examined. For instance, at pH 5.5, chalcopyrite recovery reached 81.10% while the recoveries of pyrite and pyrrhotite were 1.20% and 9.83%, respectively. Apparently, ONOS has the capacity to selectively depress pyrite and pyrrhotite flotation without affecting the flotation of chalcopyrite. In addition, it is evident that among all the three pHs examined, ONOS performance best at pH 5.5 as suggested by the largest separation window between chalcopyrite and the unwanted pyrrhotite and pyrite, in line with the work of Khoso et al. who used oxidized starch as a pyrite depressant and found that the best depression results were obtained when flotation was conducted at pH 5.5 [14]. The superior performance of ONOS at pH 5.5 may result from the strong interaction of ONOS with the pyrite and pyrrhotite surfaces. It is well known that during oxidation, the –OH groups of starch are first oxidized to –C=O groups, then to –COOH groups [30]. In acidic pHs, the surfaces of pyrite and pyrrhotite either have positive polyvalent metallic ions (Fe²⁺/Fe³⁺) or positive metal hydroxyl species (Fe(OH)⁺/Fe(OH)²⁺). A strong reaction of these species with the negatively charged functional groups (carboxylate groups) of ONOS at pH 5.5 is expected [41]. Thus, pH 5.5 was chosen for the subsequent investigations unless otherwise mentioned.

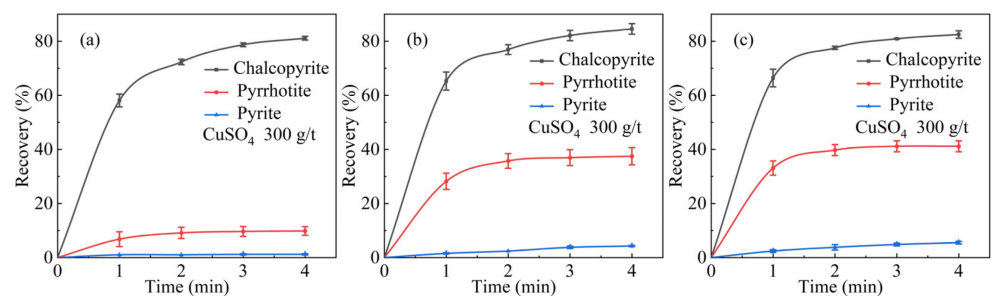


Figure 3. Flotation recovery of Cu²⁺-activated single mineral as a function of flotation time in the presence of 600 g/t ONOS at different pHs: (a) pH 5.5; (b) pH 7.0; and (c) pH 9.0.

3.2. Adsorption Tests

Figure 4 shows the adsorption results of ONOS on Cu^{2+} -activated chalcopyrite, pyrrhotite and pyrite at pH 5.5. It can be seen that the adsorption density of ONOS on the surface of the three minerals increased as the concentration of ONOS increased. Similar observations on Cu^{2+} -activated pyrite and sphalerite have previously been reported by Fletcher et al. [28] and Wei et al. [42], respectively. Importantly, the adsorption density of ONOS on the three minerals surfaces is ranked in a decreasing order as follows: pyrite > pyrrhotite > chalcopyrite. For example, at an ONOS concentration of 60 mg/L, the adsorption density of ONOS on pyrite was 4.54 mg/g, which decreased to 2.45 mg/g when pyrite was replaced by pyrrhotite and further dropped to 1.38 mg/g when chalcopyrite was the mineral examined. Based on the fact that for a specific depressant, a stronger depressant adsorption generally corresponds to a more hydrophilic mineral surface, the adsorption behaviors of ONOS on these three individual minerals are in agreement with the results of single mineral flotation where the floatability of three minerals is ranked in an increasing order as follows: pyrite < pyrrhotite < chalcopyrite. The stronger affinity of ONOS for pyrite and pyrrhotite than for chalcopyrite might be due to the fact that pyrite and pyrrhotite contain relatively higher amounts of ferric ions and ferric hydroxide species on their surfaces than chalcopyrite [29].

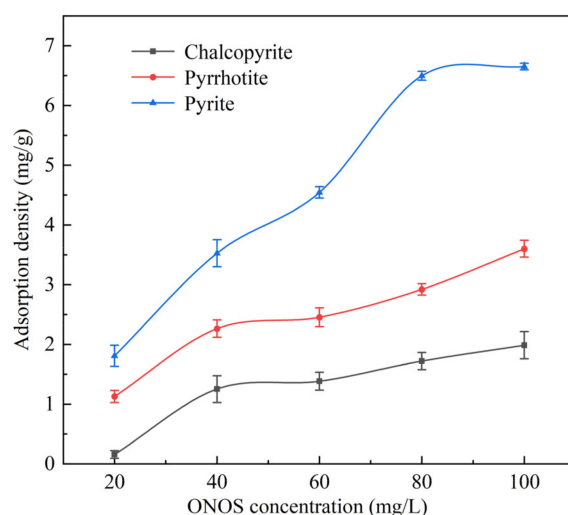


Figure 4. Adsorption density of ONOS on Cu^{2+} -activated chalcopyrite, pyrrhotite and pyrite as a function of ONOS concentration at pH 5.5. $[\text{CuSO}_4] = 3 \times 10^{-4}$ mol/L.

3.3. Zeta Potential

The zeta potentials of chalcopyrite, pyrrhotite and pyrite after Cu^{2+} activation in the presence and absence of ONOS are shown in Figure 5. It can be seen that the zeta potential of Cu^{2+} -activated chalcopyrite changed little after the addition of ONOS, suggesting that there is no strong interaction between ONOS and Cu^{2+} -activated chalcopyrite. In contrast, the zeta potentials of Cu^{2+} -activated pyrrhotite and pyrite shifted to a more negative direction after the addition of ONOS, indicating that the negative functional groups of ONOS were adsorbed on the surface of pyrrhotite and pyrite [14,15]. In summary, the zeta potential results showed the affinity of ONOS for pyrrhotite and pyrite were stronger than that for chalcopyrite, which is consistent with the flotation and adsorption results. To reveal the mechanism underpinning the selective depression performance of ONOS, XPS analysis was conducted and the results are shown in the next section.

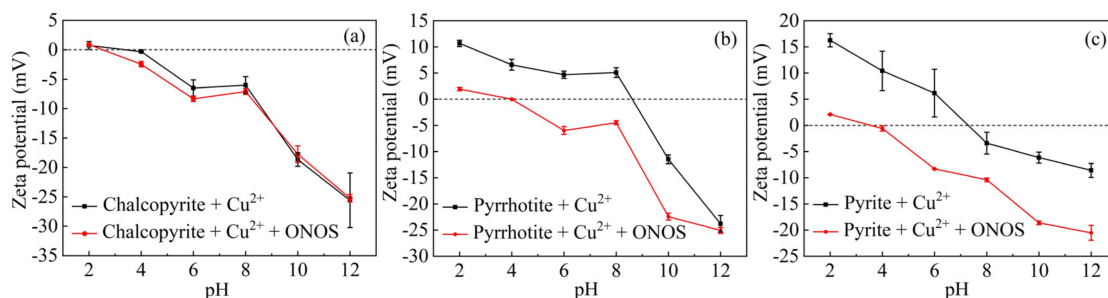


Figure 5. Zeta potential of Cu^{2+} -activated (a) chalcopyrite, (b) pyrrhotite and (c) pyrite as a function of pH in the absence and presence of 20 mg/L ONOS. $[\text{CuSO}_4] = 1 \times 10^{-4}$ mol/L.

3.4. XPS

Figure 6 shows the XPS spectra of Fe 2p, Cu 2p, O 1s for Cu^{2+} -activated pyrite in the absence and presence of ONOS. In Figure 6a, before the addition of ONOS, the peaks at 706.24 eV, 707.18 eV and 708.22 eV were attributed to Fe(II)-S [43,44]. While the peak at 710.92 eV was attributed to FeO-OH [43,45], the peak at 713.85 eV corresponded to $\text{Fe}_2(\text{SO}_4)_3$ [43,46]. After the addition of ONOS, the peaks corresponding to Fe(II)-S, FeO-OH and $\text{Fe}_2(\text{SO}_4)_3$ were all shifted, indicating the interaction of ONOS with the pyrite surface [14]. In Figure 6b, before the addition of ONOS, the peak at 530.12 eV was attributed to oxides [43,47,48]. While the peak at 531.86 eV was attributed to iron hydroxides or sulfates [48,49] and the peak at 533.46 eV was attributed to bound water [50]. After the addition of ONOS, the peak corresponding to iron hydroxides or sulfates was shifted and the peak intensity was also weakened. Meanwhile, a new peak appeared at 532.44 eV, which was due to the bonding of organic components of starch to the metal atoms on the pyrite surface (i.e., the formation of Cu(I)-ONOS complex) [23,51,52]. In Figure 6c, compared to the Cu^{2+} -activated pyrite without ONOS addition, the addition of ONOS led to a weakening of the intensity of the Cu(I)-S peak and the appearance of a new peak of copper oxide at 933.81 eV, suggesting the oxidation of Cu(I). This enhanced oxidation of Cu(I) could result from the formation of Cu(I)-biopolymer complex as suggested by Mu et al. [53]. A similar XPS observation has previously been made by Agorhom et al. [24] who used DETA to depress Cu-activated pyrite. It has been reported that Cu(I)-S is the dominant product when activating pyrite flotation using Cu^{2+} [9,54]. Owing to the presence of Cu-ONOS hydrophilic compounds as well as a reduced contribution from Cu(I)-S species, a depressed pyrite flotation was therefore expected (Figure 3) [21,24].

Figure 7 shows the XPS spectra of Fe 2p, O 1s, Cu 2p for Cu^{2+} -activated pyrrhotite in the absence and presence of ONOS. In Figure 7a, before the addition of ONOS, the peaks at 706.93 eV, 710.53 eV and 713.12 eV were attributed to Fe-S, Fe-O and $\text{Fe}_2(\text{SO}_4)_3$, respectively [55]. While the peaks at 719.71 eV and 723.93 eV corresponded to FeO-OH, the peak at 726.05 eV was the characteristic peak of hydrated iron [55]. After the addition of ONOS, the peak intensity of FeO-OH at 719.71 eV was weakened and the peak area was reduced, indicating that ONOS interacted with FeO-OH on the pyrrhotite surface [14]. In Figure 7b, the two distinct peaks at 529.63 eV and 531.53 eV before ONOS addition could belong to the iron oxides, iron hydroxides or sulfates [15,23,43]. After the addition of ONOS, similar to what occurred in the case of pyrite, a new peak appeared at 532.37 eV, which again could be attributed to the formation of Cu(I)-ONOS complex [21,24]. In Figure 7c, the Cu 2p spectra changed after the addition of ONOS. Specifically, the intensity of the Cu(I)-S peak decreased and a distinct new peak corresponded to copper oxide (Cu(II)-O) appeared at 932.32 eV, indicating that Cu(I) was oxidized to Cu(II) [24,56]. Again, this could be caused by the formation of Cu(I)-ONOS complex [21,24]. The formation of hydrophilic

Cu(I)-ONOS species and the oxidation of Cu(I) are both responsible for the depressed pyrrhotite flotation using ONOS as depressant as shown in Figure 3.

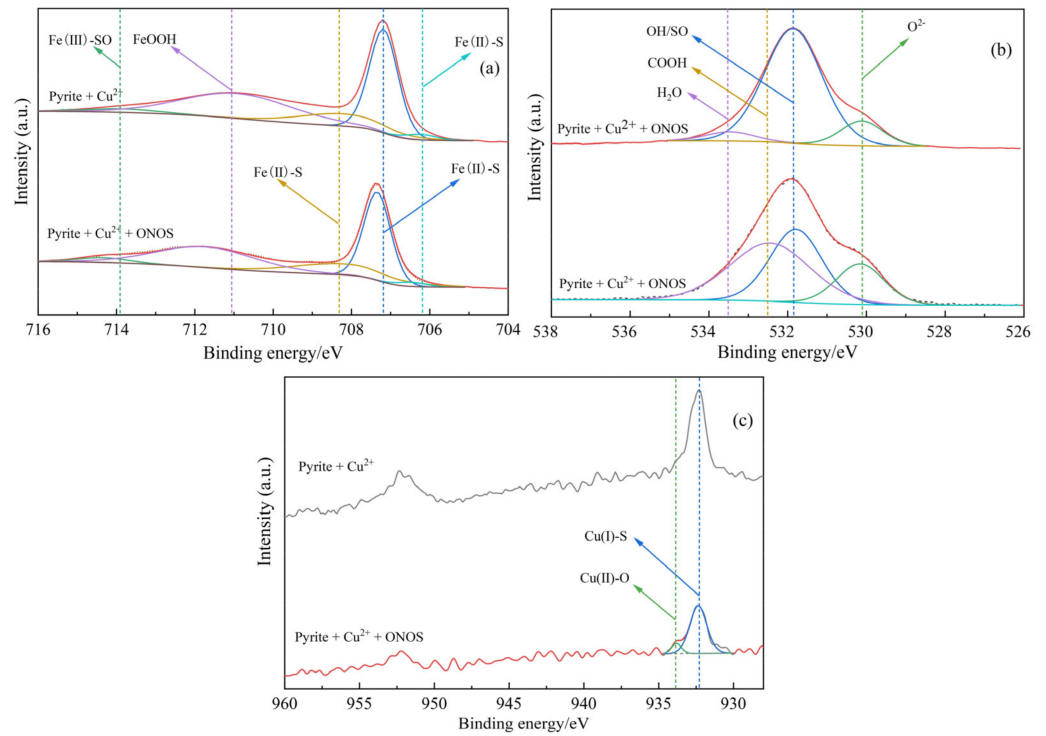


Figure 6. High resolution XPS spectra of Cu^{2+} -activated pyrite with and without ONOS addition: (a) Fe 2p; (b) O 1s; (c) Cu 2p.

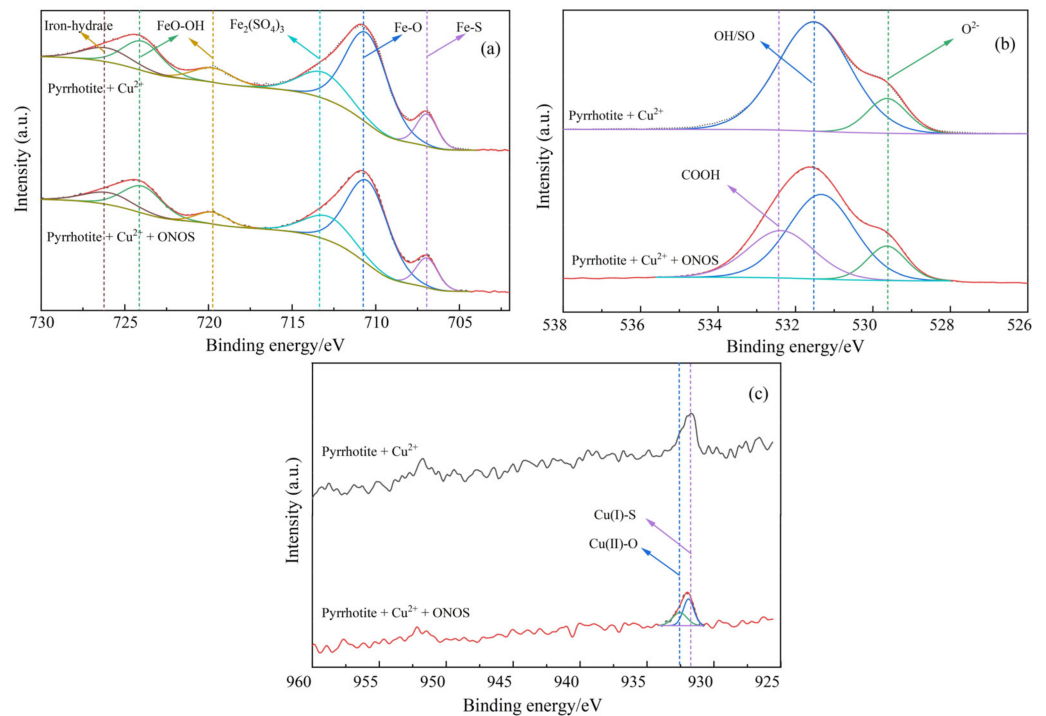


Figure 7. High resolution XPS spectra of Cu^{2+} -activated pyrrhotite with and without ONOS addition: (a) Fe 2p; (b) O 1s; (c) Cu 2p.

3.5. EDTA Extraction

EDTA was employed to extract copper oxidation products present on the surfaces of Cu^{2+} -activated pyrrhotite and pyrite before and after treatment with ONOS [57] and the results are shown in Table 3. As can be seen, the extractable copper oxidation species on the surfaces of Cu^{2+} -activated pyrrhotite and pyrite increased from 0.052 mg/g and 0.119 mg/g before treatment to 0.061 mg/g and 0.170 mg/g after treatment, respectively. This confirms the result of the XPS study and further supports the conclusion that the addition of ONOS promoted copper oxidation on the surfaces of Cu^{2+} -activated pyrrhotite and pyrite [21].

Table 3. Copper oxidation species present on the Cu^{2+} -activated mineral surfaces as extracted by EDTA with and without the addition of ONOS.

Mineral	Test Condition	Copper Oxidation Species Extracted by EDTA (mg/g of Solids)
Pyrrhotite	Cu^{2+}	0.052
	Cu^{2+} + ONOS	0.061
Pyrite	Cu^{2+}	0.119
	Cu^{2+} + ONOS	0.170

A further comparison between the amounts of EDTA extractable copper on the two minerals surfaces in the presence of ONOS revealed that the oxidation of copper on the surface of Cu^{2+} -activated pyrite was more pronounced than that on the surface of Cu^{2+} -activated pyrrhotite, which may contribute to the stronger depression of pyrite as observed in the flotation of single minerals (Figure 3).

It is worth noting that as a modified starch, ONOS belongs to the category of biomacromolecules. Hence, the formation of Cu(I)-ONOS complex may also hinder the adsorption of the xanthate collector on the pyrite and pyrrhotite surfaces, further contributing to their depression in flotation [14,53]. A schematic diagram illustrating this effect is shown in Figure 8.

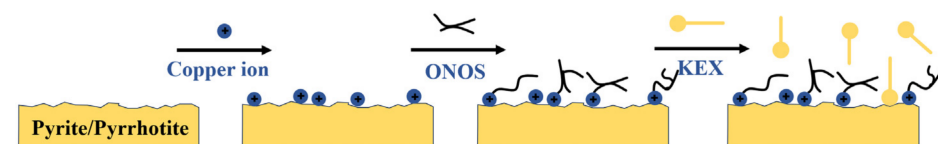


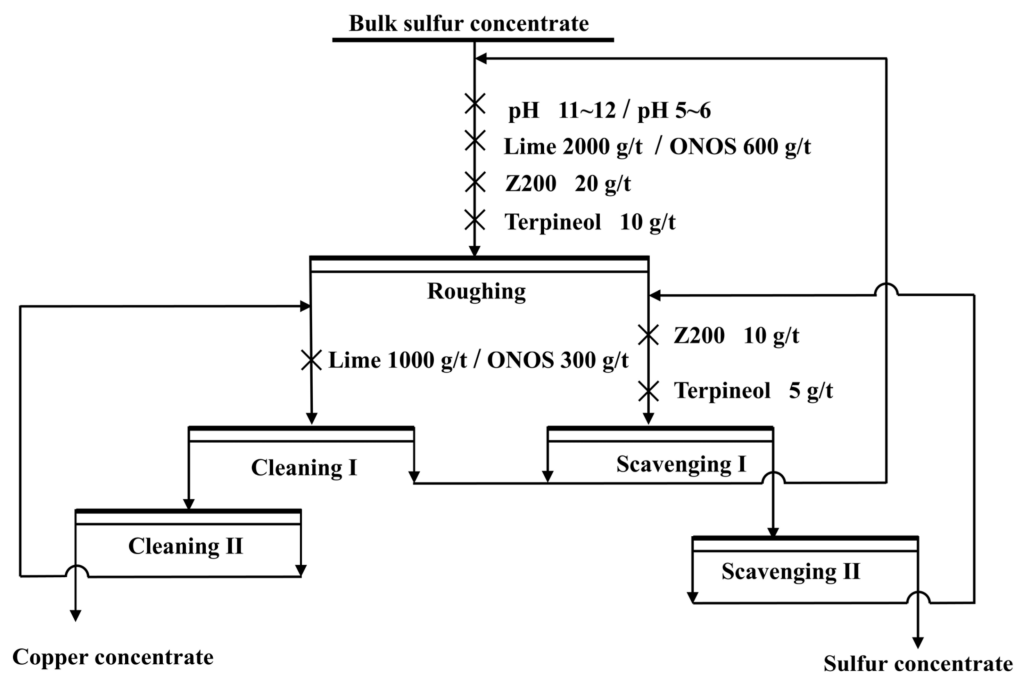
Figure 8. A competitive adsorption model of ONOS and xanthate on copper-activated pyrite and pyrrhotite surfaces.

3.6. Flotation of Bulk Sulfur Concentrate

Flotation of the bulk sulfur concentrate collected from Daye Iron Mine of WISCO using ONOS as depressant was performed to further validate the depressive capacity of ONOS, and the results were compared to those using traditional lime as depressant (Table 4). The flotation was performed according to the same flowsheet used in the mine site as shown in Figure 9.

Table 4. Flotation separation results of bulk sulfur concentrate using ONOS and lime as depressants.

Depressant	Product	Yield (%)	Cu Grade (%)	S Grade (%)	Cu Recovery (%)	S Recovery (%)
Lime	Copper concentrate	22.86	19.33	39.43	87.61	20.30
	Sulfur concentrate	77.14	0.81	45.89	12.39	79.70
	Feed	100.00	5.04	44.41	100.00	100.00
ONOS	Copper concentrate	21.97	20.66	38.59	90.37	19.06
	Sulfur concentrate	78.03	0.62	46.13	9.63	80.94
	Feed	100.00	5.02	44.47	100.00	100.00

**Figure 9.** Flotation flowsheet of bulk sulfur concentrate from Daye Iron Mine of WISCO.

It can be seen from Table 4 that at the dosages of 600 g/t (rougher) and 300 g/t (cleaner) of ONOS, Cu grade of the copper concentrate was 20.66% and Cu recovery was 90.37%. In contrast, at the dosage of 2000 g/t (rougher) and 1000 g/t (cleaner) of lime, a Cu grade of 19.33% with a Cu recovery of 87.61% was obtained. The S grade and recovery in the final sulfur concentrate were also better when lime was replaced by low doses of ONOS.

To better compare the selective depression performance of ONOS and lime, the flotation results obtained with these two depressants are presented as copper or sulfur recovery in the concentrate versus recovery of non-copper or non-sulfur components in the tailing (Fuerstenau upgrading plots, Figure 10). It can be seen that there was no obvious difference in the selectivity of the Cu-S separation process when lime was replaced by ONOS. Hence, it was concluded that ONOS can be an alternative to the problematic lime for copper-activated pyrite and pyrrhotite depression, thanks to its environmentally friendly nature and selective depression performance comparable to that of lime.

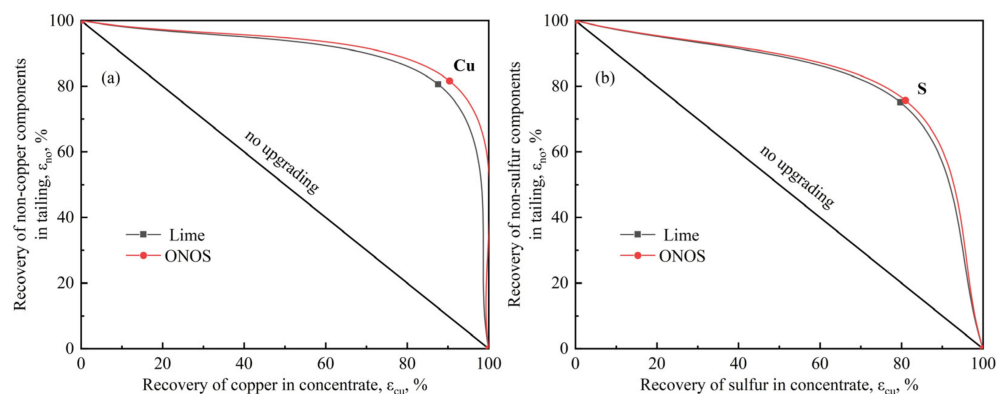


Figure 10. Copper (a) or sulfur (b) recovery in the concentrate versus recovery of non-copper or non-sulfur components in the tailing (Fuerstenau upgrading plots) using lime or ONOS as the depressant.

4. Conclusions

In this study, ONOS was examined as an eco-friendly depressant in the flotation separation of chalcopyrite from copper-activated pyrite and pyrrhotite. Micro-flotation of single minerals showed that ONOS strongly depressed copper-activated pyrite and pyrrhotite flotation while not influencing the flotation of chalcopyrite at pH 5.5. Zeta potential and adsorption results suggested that ONOS had a stronger affinity for copper-activated pyrite and pyrrhotite than for chalcopyrite, pointing to its selectivity. XPS analysis and EDTA extraction revealed that the use of ONOS led to the formation of a hydrophilic Cu(I)-ONOS complex as well as a reduction in the contribution from Cu(I)-S species, which resulted in the depressed flotation of pyrite and pyrrhotite. While flotation of an actual bulk sulfur concentrate using ONOS at a low dosage yielded slightly better Cu-S separation results, the Fuerstenau upgrading curve indicated that the selective effect of ONOS on depression of sulfur components was comparable to that of lime.

Although further testing in industrial flotation systems is needed, the results of this investigation have revealed the promising performance of ONOS in depressing copper-activated pyrite and pyrrhotite and may accelerate the application of eco-friendly depressants in chalcopyrite flotation.

Author Contributions: Conceptualization, C.H. and M.Z.; data curation, Y.L.; investigation, G.B. and C.H.; methodology, G.B.; resources, G.B. and Y.L.; supervision, M.Z.; validation, C.H.; writing—original draft, G.B.; writing—review and editing, Y.L. All authors have read and agreed to the published version of the manuscript.

Funding: This research received no external funding.

Data Availability Statement: The raw data supporting the conclusions of this article will be made available by the authors on request.

Conflicts of Interest: G.B. and C.H. are employed by WISCO Resources Group. The remaining authors declare that the research was conducted in the absence of any commercial or financial relationships that could be construed as a potential conflict of interest.

References

1. Dana, C.D.P.; Agangi, A.; Idrus, A.; Chelle-Michou, C.; Lai, C.-K.; Ishida, M.; Guillong, M.; González-Álvarez, I.; Takahashi, R.; Yano, M.; et al. The age and origin of the ruwai polymetallic skarn deposit, Indonesia: Evidence of cretaceous mineralization in the central borneo metallogenic belt. *Econ. Geol.* **2023**, *118*, 1341. [\[CrossRef\]](#)
2. Yuan, Q.; Mei, G.; Liu, C.; Cheng, Q.; Yang, S. A novel sulfur-containing ionic liquid collector for the reverse flotation separation of pyrrhotite from magnetite. *Sep. Purif. Technol.* **2022**, *303*, 122189. [\[CrossRef\]](#)
3. Arvidson, B.; Klemetti, M.; Knuutinen, T.; Kuusisto, M.; Man, Y.T. Hughes-Narborough, Flotation of pyrrhotite to produce magnetite concentrates with a sulphur level below 0.05% w/w. *Miner. Eng.* **2013**, *50*, 4–12. [\[CrossRef\]](#)

4. Miller, J.D.; Li, J.; Davidtz, J.C.; Vos, F. A review of pyrrhotite flotation chemistry in the processing of PGM ores. *Miner. Eng.* **2005**, *18*, 855. [[CrossRef](#)]
5. Khmeleva, T.N.; Skinner, W.; Beattie, D.A.; Georgiev, T. The effect of sulphite on the xanthate-induced flotation of copper-activated pyrite. *Physicochem. Probl. Miner. Process.* **2002**, *36*, 185.
6. Leppinen, J.O. FTIR and flotation investigation of the adsorption of ethyl xanthate on activated and non-activated sulfide minerals. *Int. J. Miner. Process.* **1990**, *30*, 245. [[CrossRef](#)]
7. Feng, Q.; Lu, W.; Wang, H.; Zhang, Q. Mechanistic insights into stepwise activation of malachite for enhancing surface reactivity and flotation performance. *Int. J. Miner. Metall. Mater.* **2024**, *31*, 2159. [[CrossRef](#)]
8. Feng, Q.; Zhang, Y.; Zhang, G.; Han, G.; Zhao, W. A novel sulfidization system for enhancing hemimorphite flotation through Cu/Pb binary metal ions. *Int. J. Min. Sci. Technol.* **2024**, *34*, 1741. [[CrossRef](#)]
9. Weisener, C.; Gerson, A. Cu(II) adsorption mechanism on pyrite: An XAFS and XPS study. *Surf. Interface Anal.* **2000**, *30*, 454. [[CrossRef](#)]
10. Buswell, A.M.; Nicol, M.J. Some aspects of the electrochemistry of the flotation of pyrrhotite. *J. Appl. Electrochem.* **2022**, *32*, 1321.
11. Jones, C.F.; LeCount, S.; Smart, R.S.C.; White, T.J. Compositional and structural alteration of pyrrhotite surfaces in solution: XPS and XRD studies. *Appl. Surf. Sci.* **1992**, *55*, 65. [[CrossRef](#)]
12. Buckley, A.N.; Woods, R. X-ray photoelectron spectroscopy of oxidised pyrrhotite surfaces. *Appl. Surf. Sci.* **1985**, *20*, 472. [[CrossRef](#)]
13. Meng, Q.; Yuan, Z.; Du, Y.; Wang, J. Sulfuric acid pretreatment of oxidized pyrrhotite in flotation desulphurization of magnetite concentrate. *Miner. Eng.* **2023**, *203*, 108347. [[CrossRef](#)]
14. Khoso, S.A.; Hu, Y.; Liu, R.; Tian, M.; Sun, W.; Gao, Y.; Han, H.; Gao, Z. Selective depression of pyrite with a novel functionally modified biopolymer in a Cu–Fe flotation system. *Miner. Eng.* **2019**, *135*, 55. [[CrossRef](#)]
15. Khoso, S.A.; Gao, Z.; Tian, M.; Hu, Y.; Sun, W. Adsorption and depression mechanism of an environmentally friendly reagent in differential flotation of Cu–Fe sulphides. *J. Mater. Res. Technol.* **2019**, *8*, 5422. [[CrossRef](#)]
16. Feng, Q.; Yang, W.; Chang, M.; Wen, S.; Liu, D.; Han, G. Advances in depressants for flotation separation of Cu-Fe sulfide minerals at low alkalinity: A critical review. *Int. J. Miner. Metall. Mater.* **2024**, *31*, 1–17. [[CrossRef](#)]
17. Han, G.; Wen, S.; Wang, H.; Feng, Q. Effect of starch on surface properties of pyrite and chalcopyrite and its response to flotation separation at low alkalinity. *Miner. Eng.* **2019**, *143*, 106015. [[CrossRef](#)]
18. Agheli, S.; Hassanzadeh, A.; Hassas, B.V.; Hasanzadeh, M. Effect of pyrite content of feed and configuration of locked particles on rougher flotation of copper in low and high pyritic ore types. *Int. J. Min. Sci. Technol.* **2018**, *28*, 167. [[CrossRef](#)]
19. Tukul, C.; Kelebek, S. Modulation of xanthate action by sulphite ions in pyrrhotite deactivation/depression. *Int. J. Miner. Process.* **2010**, *95*, 47. [[CrossRef](#)]
20. Bıcak, O.; Ekmekçi, Z.; Bradshaw, D.; Harris, P.J. Adsorption of guar gum and CMC on pyrite. *Miner. Eng.* **2007**, *20*, 996. [[CrossRef](#)]
21. Agorhom, E.A.; Skinner, W.; Zanin, M. Post-regrind selective depression of pyrite in pyritic copper–gold flotation using aeration and diethylenetriamine. *Miner. Eng.* **2015**, *72*, 36. [[CrossRef](#)]
22. Multani, R.S.; Waters, K.E. Pyrrhotite depression studies with DETA and SMBS on a Ni-Cu sulphide ore. *Can. J. Chem. Eng.* **2019**, *97*, 2121. [[CrossRef](#)]
23. Gonçalves, C.D.C.; Liu, Q. The effect of crosslinking additives and molecular weight of starch depressants on pyrrhotite and pentlandite floatabilities. *Miner. Eng.* **2022**, *180*, 107489.
24. Agorhom, E.A.; Skinner, W.; Zanin, M. Diethylenetriamine depression of Cu-activated pyrite hydrophobised by xanthate. *Miner. Eng.* **2014**, *57*, 36. [[CrossRef](#)]
25. Gonçalves, C.D.C.; Bobicki, E.R.; Liu, Q. Insight on the mechanism of hexagonal pyrrhotite depression by starch during flotation. *Miner. Eng.* **2023**, *203*, 108335.
26. Furnell, E.; Tian, X.; Bobicki, E.R. Diethylenetriamine as a selective pyrrhotite depressant: Properties, application, and mitigation strategies. *Can. J. Chem. Eng.* **2021**, *99*, 1316. [[CrossRef](#)]
27. Junejo, S.A.; Flanagan, B.M.; Zhang, B.; Dhital, S. Starch structure and nutritional functionality—Past revelations and future prospects. *Carbohydr. Polym.* **2022**, *277*, 118837. [[CrossRef](#)]
28. Fletcher, B.; Chimonyo, W.; Peng, Y. A comparison of native starch, oxidized starch and CMC as copper-activated pyrite depressants. *Miner. Eng.* **2020**, *156*, 106532. [[CrossRef](#)]
29. Khoso, S.A.; Lyu, F.; Meng, X.; Hu, Y.; Sun, W. Selective separation of chalcopyrite and pyrite with a novel and non-hazardous depressant reagent scheme. *Chem. Eng. Sci.* **2019**, *209*, 115204. [[CrossRef](#)]
30. Chapagai, M.K.; Fletcher, B.; Gidley, M.J. Characterization of structure-function properties relevant to copper-activated pyrite depression by different starches. *Carbohydr. Polym.* **2023**, *312*, 120841. [[CrossRef](#)]
31. May, F.; Gock, E.; Vogt, V.; Brüser, V. Plasma-modification of sulfides for optimizing froth-flotation properties. *Miner. Eng.* **2012**, *35*, 67. [[CrossRef](#)]

32. Silva, L.M.D.; Jardim, W.D.F. Trends and strategies of ozone application in environmental problems. *Quim. Nova* **2006**, *29*, 310. [[CrossRef](#)]
33. Devatkal, S.K.; Kumar, C.; Juneja, V.; Inbaraj, S. Effect of aqueous ozone on inactivation of bacteria isolated from the meat products and equipment. *Biologia* **2023**, *78*, 3295. [[CrossRef](#)]
34. Zhang, M.; Xu, Z.; Zhang, Q.; Dan, Z.; Fu, H.; Yao, W. Properties and potential application of ozone-oxidized starch for enhanced reverse flotation of fine hematite. *Miner. Eng.* **2023**, *198*, 108084. [[CrossRef](#)]
35. Hewage, S.A.; Batagoda, J.H.; Meegoda, J.N. In situ remediation of sediments contaminated with organic pollutants using ultrasound and ozone nanobubbles. *Environ. Eng. Sci.* **2020**, *37*, 521.
36. Takahashi, M.; Ishikawa, H.; Asano, T.; Horibe, H. Effect of Microbubbles on Ozonized Water for Photoresist Removal. *J. Phys. Chem. C* **2012**, *116*, 12578. [[CrossRef](#)]
37. Li, Y.; Zhang, M.; Fan, R. Selective flotation separation of molybdenite from chalcopyrite by ozone nanobubbles preconditioning. *Sep. Purif. Technol.* **2025**, *359*, 130507. [[CrossRef](#)]
38. Dubois, M.; Gilles, K.A.; Hamilton, J.K.; Rebers, P.A.; Smooth, F. Colorimetric method for determination of sugars and related substances. *Anal. Chem.* **1956**, *28*, 350. [[CrossRef](#)]
39. Peng, Y.; Grano, S. Effect of grinding media on the activation of pyrite flotation. *Miner. Eng.* **2010**, *23*, 600. [[CrossRef](#)]
40. Dichmann, T.K.; Finch, J.A. The role of copper ions in sphalerite-pyrite flotation selectivity. *Miner. Eng.* **2001**, *14*, 217. [[CrossRef](#)]
41. Khoso, S.A.; Hu, Y.; Tian, M.; Gao, Z.; Sun, W. Evaluation of green synthetic depressants for sulfide flotation: Synthesis, characterization and floatation performance to pyrite and chalcopyrite. *Sep. Purif. Technol.* **2021**, *259*, 118138. [[CrossRef](#)]
42. Wei, M.; Lv, J.; Kong, L.; Tong, X. Differential depression and mechanism of copper ion-activated sphalerite with wheat starch and rice starch as flotation depressants. *Adv. Powder Technol.* **2024**, *35*, 104446. [[CrossRef](#)]
43. Li, W.; Li, Y.; Wu, X.; Wang, Z.; Wei, Z. Pyrite activation in seawater flotation by copper and lead ions: XPS and in-situ electrochemical investigation. *Appl. Surf. Sci.* **2025**, *680*, 161363. [[CrossRef](#)]
44. Nesbitt, H.W.; Muir, I.J. X-ray photoelectron spectroscopic study of a pristine pyrite surface reacted with water vapour and air. *Geochim. Cosmochim.* **1994**, *58*, 4667. [[CrossRef](#)]
45. Konno, H.; Nagayama, M. X-ray photoelectron spectra of hexavalent iron. *J. Electron Spectrosc. Relat. Phenom.* **1980**, *18*, 341. [[CrossRef](#)]
46. Cai, Y.; Pan, Y.; Xue, J.; Sun, Q.; Su, G.; Li, X. Comparative XPS study between experimentally and naturally weathered pyrites. *Appl. Surf. Sci.* **2009**, *255*, 8750. [[CrossRef](#)]
47. Buckley, A.N.; Goh, S.W.; Lamb, R.N.; Woods, R. Interaction of thiol collectors with pre-oxidised sulfide minerals. *Int. J. Miner. Process.* **2003**, *72*, 163. [[CrossRef](#)]
48. Nesbitt, H.W.; Bancroft, G.M.; Pratt, A.R.; Scaini, M.J. Sulfur and iron surface states on fractured pyrite surfaces. *Am. Mineral.* **1998**, *83*, 1067. [[CrossRef](#)]
49. Harmer, S.L.; Mierczynska-Vasilev, A.; Beattie, D.A.; Shapter, J.G. The effect of bulk iron concentration and heterogeneities on the copper activation of sphalerite. *Miner. Eng.* **2008**, *21*, 1005. [[CrossRef](#)]
50. Nesbitt, H.W.; Muir, I.J. Oxidation states and speciation of secondary products on pyrite and arsenopyrite reacted with mine waste waters and air. *Mineral. Petrol.* **1998**, *62*, 123. [[CrossRef](#)]
51. Biesinger, M.C.; Lau, L.W.M.; Gerson, A.R.; Smart, R.S.C. Resolving surface chemical states in XPS analysis of first row transition metals, oxides and hydroxides: Sc, Ti, V, Cu and Zn. *Appl. Surf. Sci.* **2010**, *257*, 887. [[CrossRef](#)]
52. Moreira, G.F.; Peçanha, E.R.; Monte, M.B.M.; Filho, L.S.L.; Stavale, F. XPS study on the mechanism of starch-hematite surface chemical complexation. *Miner. Eng.* **2017**, *110*, 96. [[CrossRef](#)]
53. Mu, Y.; Peng, Y.; Lauten, R.A. The depression of copper-activated pyrite in flotation by biopolymers with different compositions. *Miner. Eng.* **2016**, *96–97*, 113. [[CrossRef](#)]
54. Chandra, A.P.; Puskar, L.; Simpson, D.J.; Gerson, A.R. Copper and xanthate adsorption onto pyrite surfaces: Implications for mineral separation through flotation. *Int. J. Miner. Process.* **2012**, *114*, 16–26. [[CrossRef](#)]
55. Qiu, T.; Ding, K.; Yan, H.; Yang, L.; Wu, H.; Zhao, G.; Qiu, X. Electrochemistry and DFT study of galvanic interaction on the surface of monoclinic pyrrhotite (0 0 1) and galena (1 0 0). *Int. J. Min. Sci. Technol.* **2024**, *34*, 1151. [[CrossRef](#)]
56. Peng, W.; Liu, S.; Cao, Y.; Wang, W.; Lv, S.; Huang, Y. A novel approach for selective flotation separation of chalcopyrite and molybdenite—Electrocatalytic oxidation pretreatment and its mechanism. *Appl. Surf. Sci.* **2022**, *597*, 153753. [[CrossRef](#)]
57. Lee, R.L.J.; Peng, Y. Assessing the depression of high-concentration pyrite in copper flotation by high pH. *Miner. Eng.* **2024**, *209*, 108651.

Disclaimer/Publisher’s Note: The statements, opinions and data contained in all publications are solely those of the individual author(s) and contributor(s) and not of MDPI and/or the editor(s). MDPI and/or the editor(s) disclaim responsibility for any injury to people or property resulting from any ideas, methods, instructions or products referred to in the content.